European Review for Medical and Pharmacological Sciences 2020; 24: 7063-7076

In vitro redox activity of haemozoin and β-haemozoin interacting with the following antimalarials: artemether, lumefantrine and quinine

J.L. IMBERT PALAFOX[1], L. GONZÁLEZ LINARES[1], V.E. REYES-CRUZ[2], M.A. BECERRIL FLORES[1], J.C. RUVALCABA LEDEZMA[1], C.M. GONZALEZ ALVAREZ[3], A. ARENAS FLORES[2], J.E. BAUTISTA GARCIA[1]

[1]Área Académica Medicina, Instituto de Ciencias de la Salud, Universidad Autónoma del Estado de Hidalgo, Pachuca, Estado de Hidalgo, México
[2]Área Académica Ciencias de la Tierra, Materiales, Metalurgia, Instituto de Ciencias Básicas e Ingeniería, Universidad Autónoma del Estado de Hidalgo, Pachuca, Estado de Hidalgo, México
[3]Facultad de Ciencias Químicas, Benemérita Universidad Autónoma de Puebla, Puebla, México

Abstract. – OBJECTIVE: Malaria parasites invade, grow and multiply inside erythrocytes and obtain nourishment from haemoglobin. Then, the released haem group is oxidized to haematin and inert dimeric haemozoin bio-crystals form, which provides the parasite a unique way to avoid the toxicity associated with the haem group. Therefore, antimalarial drugs are designed to inhibit dimer formation; however, recent electrochemical studies indicate that an inert dimer also promotes a toxic oxidizing environment. Therefore, this work explores drug reactivity in the presence of monomers and dimers to evaluate their contribution to redox activity.

MATERIALS AND METHODS: Three medicines mixed with haemozoin or β-haemozoin in carbon paste electrodes were tested using cyclic voltammetry.

RESULTS: The data indicated again that the substances modify the natural redox state of haemozoin and β-haemozoin. This effect could be attributed to the natural oxidation potential of the drugs. In addition, it was found that the oxidation potential decreased through quinine, lumefantrine and artemether with the same tendency in the presence of haemozoin but with less current density. Additionally, it was observed that the oxidation response between the monomer haemozoin and antimalarial drugs is carried out at more negative potentials.

CONCLUSIONS: Together, the total results indicate that antimalarials per se can contribute to oxidation processes and that in combination with monomeric or dimeric haemozoin can increase or decrease the oxidizing power of the haemozoin forms. The various oxidizing environments suggest that the cell membranes can also be damaged by the unique presence of the antimalarial.

Key Words:
Haemozoin, β-Haemozoin, Antimalarials, Cyclic Voltammetry, *Meccus longipennis*.

Introduction

Resistance to new antimalarial drugs has become a research priority, and haemozoin inhibition is a very attractive target because it appears to be an immutable pathway[1]. Due to an incomplete understanding of the parasite processes that lead to haemozoin formation[2-4] a drug that specifically targets the parasite factors responsible for their production has not yet been developed; thus, the topic has been a subject of intense debate. Although a protein to detoxify the haem group (haem detoxifying protein) has been identified and characterized in *Plasmodium falciparum*, which is critical for the survival of the parasite, the systematic degradation of haemoglobin, the release of the haem group and the formation of haemozoin [Hz] are not completely clear. Under this view, if HDP can be an important contributor in achieving non-toxic Hz levels found in the parasite, experimental support by classical molecular, biochemical and cell biological approaches[5] will be required.

Corresponding Author: Jose Luis Imbert Palafox, MD; e-mail: imbertox@hotmail.com

The haematophagous hemipteran *Rhodnius prolixus* or *Meccus longipennis*, such as *Plasmodium,* have evolved many genetic resources to protect cells against haem toxicity. In this sense, haemoglobin degradation in *Triatominae* insects is also a complex biochemical process, which takes place in an environment apparently different from a digestive vacuole[6-9].

The formation of a haemozoin-like crystallite is a vital process of insect vectors of Chagas disease[10,11], *Schistosomiasis*[12,13] and probably other diseases transmitted by the genus of haematophagous mosquitoes, such as *Aedes*, *Anopheles or Lutzomia*. Notably, once the blood meal of the insect is digested in the stomach or anterior midgut, the haemoglobin is denatured, and then, the haem group is free to pass to the small intestine or posterior midgut space where it is polymerized as nontoxic haemozoin[6,10,11].

These apparently small and irregular fragments that are found adhered to intestinal cells provide strong evidence that Hz formation in *Rhodnius prolixus* or haematophagous insects is a very efficient process and that haem crystallization favorably occurs[10,11,14], in spite of the fact that the stomach and intestines are not a big digestive vacuole.

Although the physical-chemical environments are likely to be similar, the crystallization processes of haematin in these insects are apparently not the same; thus, the basic requirements of the redox balance and pH equilibrium between the lipidic or aqueous medium may be similar from a biochemical point of view[15,16]. However, in the faeces of these bugs, uniform crystallites do not occur, such as those observed in malaria samples; interestingly, crystalline micro-arrays are produced with remarkable uniformity in morphology and size in malaria samples[17-19].

The first description of Hz in a different organism from *Plasmodium* claims that "after a blood meal, *R. prolixus* midgut presents a huge amount of Hz granules"; the midgut lumen contains large electron-dense aggregates similar in appearance to the haemozoin granules found in malaria parasites[10,11]. The process of Hz formation in *S. mansoni* and *R. prolixus* is similar[14], but the differences do not seem to be derived from distinct atomic structures; instead, they are generated from the crystal growth conditions. Thus, in part, this issue was elegantly resolved and showed that the haem crystals of the insect share the same unit cell and structure[14]. It has been challenging to reconcile the observations or experimental evidence of inert haemozoin crystals embedded within a lipid nanosphere with those of their pro-oxidant effects and how the haem group avoids oxidation[15,16,20,21]; therefore, this research has the principal aim of determining whether there is a possible potential generation of oxidative stress or an unbalanced redox state due to the interaction of antimalarial drugs with Hz or β-Hz in a similar osmolar medium.

The subsidiary aims of the study are to understand and know more about the toxicity and instability aspects and explore whether antimalarial drugs may have potential secondary effects, such as ROS generation[21].

Materials and Methods

Reagents and Drugs

The reactive substances were analytical grade-high purity and the deionised water had a specific resistance of 18.2 MΩcm^{-1}. Protoporphyrin IX®, (PPIX), ($C_{34}H_{34}N_4O_4$, MW 562.7) approx. ≥ 95%, catalog P8293; Quinine, (QN), ($C_{20}H_{24}N_2O_2$, MW 324.42) approx. 90%, catalog 145904; Amodiaquine, (AQ), ($C_{20}H_{22}ClN_3O$*2HCl $2H_2O$, MW 464.8) approx. ≥ 99%, catalog A2799; Chloroquine, (CQ), ($C_{18}H_{26}ClN_3$ $2H_3PO_4$, MW 515.86) approx. ≥ 99%, catalog C6628; Sodium Azide (NaN_3, MW 65.01) approx. 99.5%; Sodium hydroxide (NaOH, MW 40) approx. 98% and Silicon oil (SiO) (C_7H_8OSi, MW 136.22) approx. ≥ 99%, [the binding agent with 0.963 g/mL density and 200 cSt viscosity at (25°C)] all of them were obtained from Sigma-Aldrich (St. Louis, MO, USA). Arthemeter, (ART), ($C_{12}H_{26}O_5$, MW 298.4) approx. ≥ 99% and Lumefantrine, (LF), ($C_{30}H_{32}O_1N_{14}Cl_3$, MW 298.4) approx. ≥ 99% were obtained from Novartis Pharma AG (Campus Basel, Switzerland). Sodium chloride (NaCl, MW 58.44) 100.2%; Sodium nitrate ($NaNO_3$, MW 84.999) 100.7%; Hydrochloric acid (HCl, MW 36.46) 35.5-38%; Absolute ethylic alcohol (C_2H_5OH, MW 46.07) 99.5% and Ethylenediaminetetraacetic acid (EDTA, $C_{10}H_{16}N_2O_8$, MW 292.25) approx. 99.4% were obtained from J. T. Baker (Phillipsburg, NJ, USA). Graphite powder, 2-15 μm particle size, (C, MW 15.9999) approx. 99.9995%, Alfa Aesar™ (Thermo Fisher Scientific, Waltham, MA; USA). Hemoglobin, (Hb), (MW 64 kDa) approx ≥ 99% Becton & Dickinson (Franklin Lakes, NJ, USA). Haemozoin (Hz, *Meccus longipennis*), ($C_{34}H_{33}FeN_4O_5$, MW 633.50) approx. ≥50% and β-Haemozoin

(β-Hz, *Meccus longipennis*), ($C_{68}H_{66}Fe_2N_8O_{10}$, MW 1264.00) approx. ≥50% were obtained from AAM-ICSA-UAEH, the present work.

Hz and β-Hz Preparation from M. Longipennis

The techniques used were similar to references[22,23]. Briefly, 2.1 g of insect faeces and urine were collected. The material was pulverized, and then, dialyzed against water. After centrifugation at 2,500 rpm for 20 min, the dark supernatant was filtered (Whatman® grade I, catalogue No. 1001 125), and then, mixed with 1 M NaOH to obtain soluble Hz. To obtain β-Hz, the solution was acidified with concentrated HCl, and the brownish precipitate was stored for 24 hours. Then, the pellet was centrifuged at 2,500 rpm for 20 min and washed with deionized water (pH=6.0) 5 to 8 times. Finally, the β-Hz nano-crystals and micro-crystals were separated from the water and allowed to dry at 32°C. Approximately 1.2 g of pure substance were obtained, representing 57% of the original sample.

Preparation of Controls HZ and β-HZ from Hemoglobin of B&D®

The methods used were similar to references[22,23].

Characterization by Infrared and UV-Visible Spectrophotometry

To perform the FTIR spectra and the spectral studies in UV-visible range, the methods used were similar to references[22,23]. Results show the average from three determinations for obtaining statistical significance.

Characterization by Zeta Potential

The Hz from *M. longipennis* 0.1 M, was dissolved in deionized water and after that was realized the pH adjustment with NaOH 0.1 M or HCl 0.1 M for obtaining pH values of 4, 5, 6, 7, 8 and 9 and the Z potential in a 0 to -35 mV range was determined. The equipment used was a Zetasizer, Brand Malvern, Model 3000 HSA and results show the average of six determinations for each pH[23].

Characterization through SEM, EDS and XRD

For Electron Micrograph and Energy Spectrum of Hz and β-Hz molecules from *M. longipennis*, the equipment used was a JEOL 6300 Scanning Electronic Microscope, equipped with Energy Dispersive Spectrometer. Were used secondary electrons in 20 to 30 kV range and amplification were of 5,500X for obtaining topographical images. The retro dispersal electrons were from k level for microanalysis detecting the percentual weight of Elements (%) in a point area (100 nm^2) at 30 Kv, field depth 0.3 mm, ×10,000 times in 60 s.

The X-ray diffraction powder pattern was obtained in equipment Inel, Equinox 2000. XRD analysis was performed with CoKα1 X-rays, a step size of 0.02 and collection time of 1 s across a 2θ range of 20-50º. The diffraction spectra were processed using X'Pert High Score (Version 2.0) software with reference to the Powder Diffraction File database (Version 4þ 2009) from the International Centre for Diffraction Data (Newton Square, PA, USA)[23].

Electrolytic Solutions, Electrochemical Cell and Working Electrodes

The first solution was 0.1 M $NaNO_3$, pH 6.50 and second one was 0.15 M NaCl, pH 6.65; a typical Pyrex brand cell was used, with three electrodes at room temperature and Nitrogen gas, the auxiliary or Opposite-Electrode was a graphite bar. The Reference-Electrode was sulphates saturated (SSE) $Hg/Hg_2SO_4(s)/K_2SO_4$ (sat), immerse in a "Luggin" capillary tube[22].

All values of electrochemical assays were converted and reported using the Standard Hydrogen Electrode scale (SHE, 0.615 V total sum). The values of the electric current density were reported making a quotient between current flow and the Work-Electrode transversal surface work area (0.0314 cm^2).

Buffers for pH regulation were not used because the voltammetry assays were in micro-electrolysis conditions, and the changes were not appreciable.

In order to obtain reliable results and to assure the reproducibility of the voltammetry responses, it was used the Open Circuit Potential (OCP) or Null Current (NC), and it was determined by following the Potential Variation Rate in function of time, until reaching a stable stationary state after being in contact with the solution.

All the voltammetry assays were started with a specific (OCP) and scanning velocity (ν) of 20 mVs^{-1} and the electro activity interval was established between -1.5 and 2.0 V. The potential window for the NaCl medium was established between two intervals of -1.5 to 2.0 V and -0.36 to 1.6 V.

The Carbon Paste Electrodes (CPE) were prepared with different compounds: Hz and β-Hz

controls prepared from Becton & Dickinson®, Hz and β-Hz from *M. longipennis* alone or mixed with antimalarial drugs and complemented with Graphite powder and Silicon oil. The composition was: graphite, sample (Hz or β-Hz) or drug and silicon oil, and the weight proportions (wt.) were graphite: sample 50:50; graphite: drug 50:50; graphite: sample: drug 50:25:25. Two additional were: graphite: sample: drug 50:17:33 and 50:13:37 all the CPE were completed with 0.3 ml oil[22].

The determinations were realized with a Potenciostat-Galvanostat, Mark PAR, Model 263A online with a Personal Computer and the runs, determinations, conditions and graphical steps were registered with the software Power Suite Version 3.1[22].

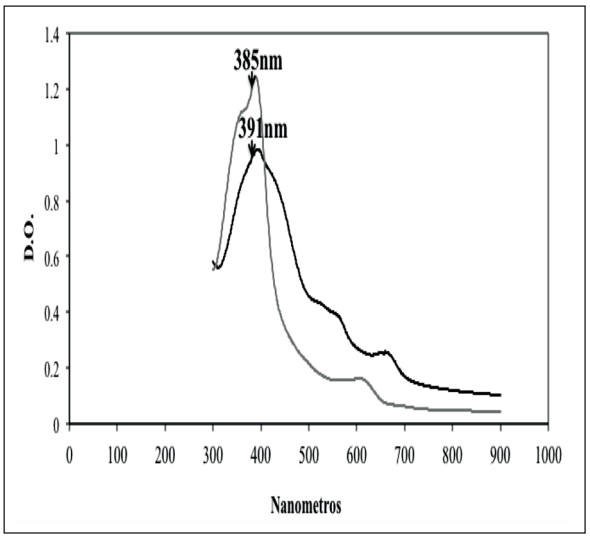

Figure 2. Absorption spectra of Hz (Grey line) and β-Hz (Black line) from *M. longipennis*.

Results

FTIR and UV-Visible Spectra

Figure 1 shows the infrared spectra for *M. longipennis,* where the classic bands corresponding to carbonyl (C=O) and carboxylate (C-O) are observed at 1671 and 1127 cm^{-1} for Hz and at 1651 and 1046 cm^{-1} for β-Hz; the signals match those in the literature[10,11,24-26]. The absorption spectra of Hz and β-Hz from *M. longipennis* in Figure 2 show the classical shift of the Söret band. The band displacement, from 391 nm in an alkaline solution to 384 nm in an acidic medium, is due to the iron movement in the porphyrin plane, which is similar to what was reported in the literature and confirms two different chemical structures.

Zeta Potential

In the curves of Figure 3, two slopes higher than 90^0 can be observed between a pH interval of 4.0 to 6.0; these two curves correspond to β-Hz and the third slope at a pH interval of 6.0 to 9.0 correspond to Hz. The slopes

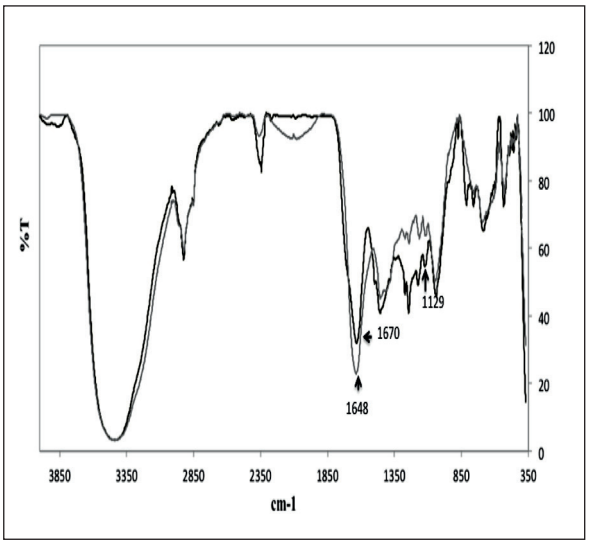

Figure 1. FTIR spectra of Hz (Black line) and β-Hz (Grey line) from *M. longipennis.*

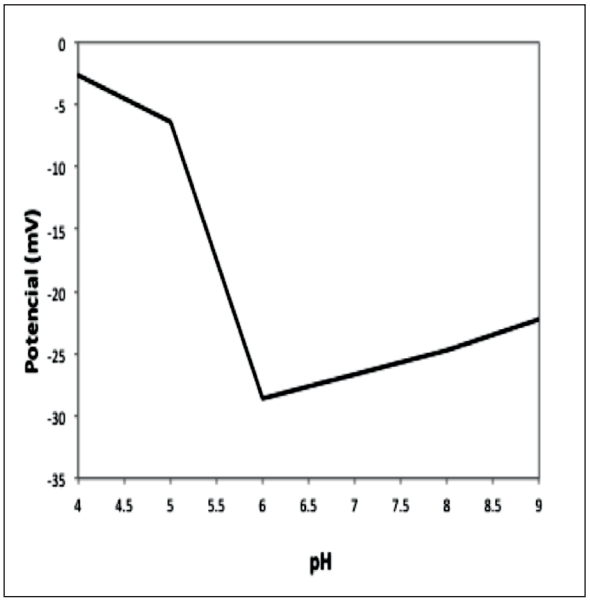

Figure 3. Zeta potential of Hz and β-Hz from *M. longipennis.*

have a negative surface charge for the Hz-βHz conjugated pair; the first one has a minor or attenuating change from -23 mV towards a negative potential close to -30 mV in a pH range of 9.0 to 6.0. The second one occurs when the dimerization process begins. Although the molecules are not completely soluble and the pH changes to 6.0, a short predictable leap of -23 mV occurs, and the electric potential for β-Hz formation has a value of -6.0 mV and pH 5.0. The third change is when the pH changes from 5.0 to 4.0; the β-Hz molecules are less soluble, and the potential change is -6 to -3 mV. Most likely, the second and third slopes in the pH intervals of 6.0 to 5.0 and 5.0 to 4.0 show the union and microcrystallisation phases like as succeeding in the digestive vacuole of the parasite where the pH is 4.5 to 4.9[7,18,19,27]. These steps carry a notable calorific energy release in an assay titration and probably result from electrostatic repulsion and attraction and van der Waals forces (*personal observation*). The Hz and β-Hz molecules in alkaline or acidic solutions can acquire a surface electric charge, which can favor differential adsorption of ion solutions (antimalarials, for example) on the surface. The above adsorption affects the ion distribution and increases the concentration of counterions, thus forming a double electric layer at the interface. The internal region includes ions strongly bound to the surface, and at the outer region, the ion distribution is determined by the balance between electrostatic forces and thermal movement. Therefore, the potential decreases when increasing the distance from the surface to a sufficiently large distance and thus achieves the solution zero potential. This potential reflects the effective charge on the particles and correlates with the electrostatic repulsion between them.

Surprisingly, the negative surface charge of the dimeric molecules reaches the values of -6.0 mV and -3.0 mV, which are close to electrical neutrality. This may mean that additional carboxyl group protonation occurs at pH values of 4.0 to 5.0.

Microscopical Description

Figure 4 shows the control compounds obtained from Haemoglobin® B&D using a USB M-1 microscope (Cole-Parmer, amplified (×200)). Characteristic brown and crystalline aspects can be observed. Additionally, Hz has a large homogeneous crystalline form and β-Hz presents a very small agglomerating particle.

Figure 5 shows the micrographs of Hz and β-Hz crystals obtained from *M. longipennis*. In Figure 5A, there are many small plane crystals, thin needle-like structures and the presence of several particle sizes with average dimensions of 2 μm × 4-5 μm. The β-Hz image in Figure

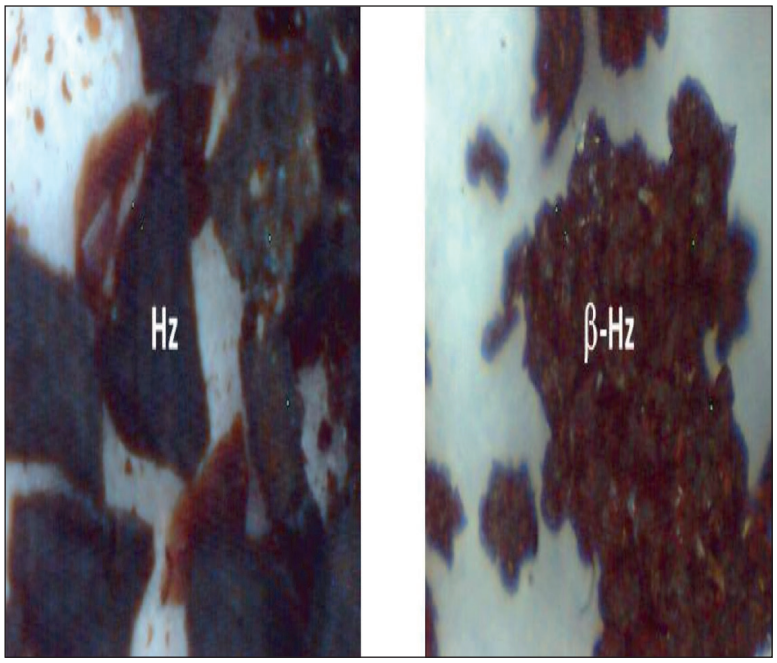

Figure 4. Hz (a) and β-Hz crystals (b) obtained of Hemoglobine® Beckton and Dickinson.

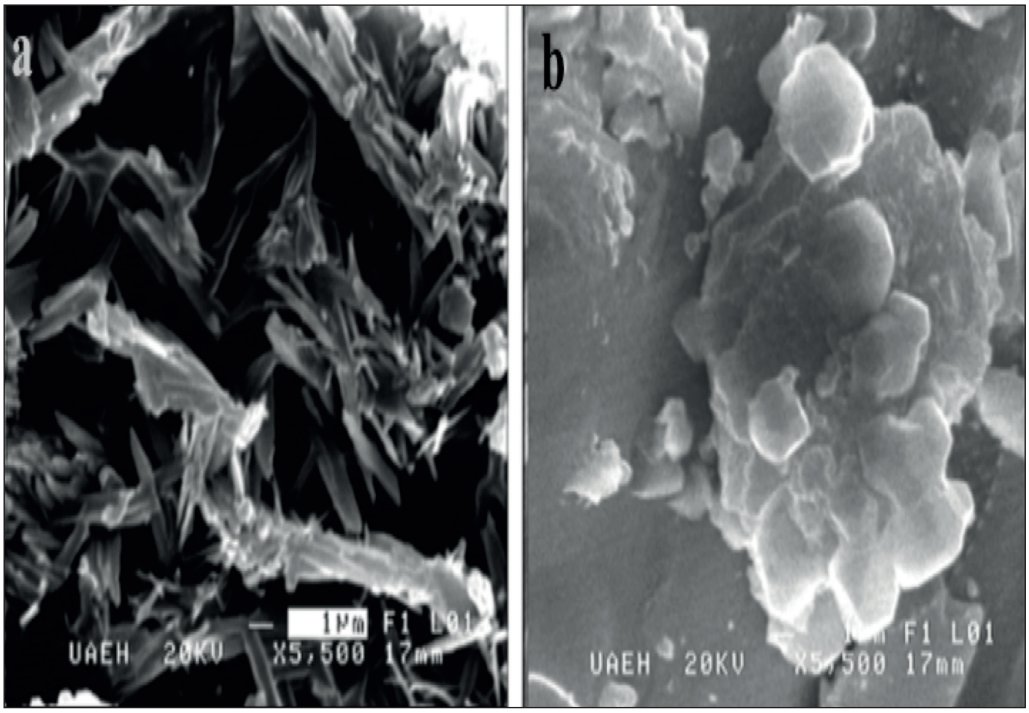

Figure 5. SEM of **A,** Hz and **B,** β-Hz crystals from *M. longipennis.* Magnification 5, 500 ×, bar 1mm.

5B shows crystalline agglomerates with more homogeneous particle sizes that have cubic dimensions of 2 µm × 2 µm × 2 µm. Furthermore, the crystals in Figure 5B are in large 3D agglomerates, and the geometrical shape includes flat and well-formed faces with straight edges and sharp vertices. In both samples uric acid remains were not observed and the sample collection method was considered adequate.

Atomic and Molecular Spectroscopic Description

EDS tests for the Hz and β-Hz from the *M. longipennis* samples are shown in Figure 6. The

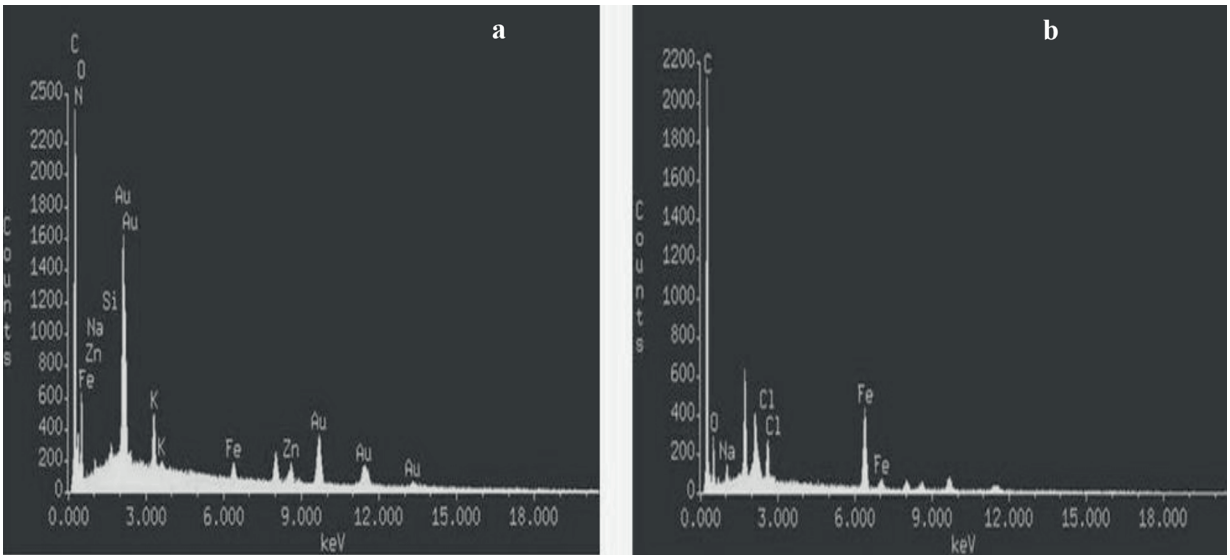

Figure 6. Elemental microanalysis of iron in Hz **(a)** and β-Hz **(b)** by EDS and XRS.

Table I. Elemental microanalysis with Scanning Energy Dispersive by X Ray (SED) from *M. longipennis* samples.

Element	This work		Reference (20)	
	Hz	ß-Hz	Hz	ß-Hz
Iron (Fe)	0.54	4.57	0.36	2.38
Carbon (C)	37.44	52.32	34.21	38.13
Nitrogen (N)	24.59	20.26	29.35	21.03
Natrium (Na)	0.35	1	0.02	0.44
Chloride (Cl)	0	0.92	0.05	1.43
Oxygen (O)	23.59	20.93	35.93	35.07
Total	86.51	100	99.92	98.48

samples are visualized through secondary electrons at 20KV 20KV, working distance of 17mm, and at a 5,500×magnification.

Elemental microanalyses of the same molecules by X-ray spectroscopy and energy dispersive spectroscopy show the major signal for iron (Fe) in Hz (Figure 6A) and β-Hz (Figure 6B). The associated bands of gold (Au) resulted from the coating process, and chloride and sodium were contaminants from solutions employed for their purification. With respect to the iron composition, the β-Hz has a concentration 8.46 times greater than Hz from *M. longipennis* (Table I), and this difference in content in the dimer and monomer forms show the sample purity and efficiency in the sample collection procedure. It can be observed that the Hz and β-Hz amounts obtained from insect faeces are high, despite being in small amounts of sample, which is contrary to the great amount of pure Haemoglobin® B&D used by the chemical method. This means that the biological digestion of blood from hematophagous insects is more efficient than chemical digestion.

Crystallographic Structure

Figure 7 shows three diffraction patterns from *M. longipennis* samples: faeces, the Hz and β-Hz obtained for this study. An FCC (face centered cubic) crystalline structure with planes [1,1,1], [2,0,0], [2,2,0] and [3,1,1] can be observed from the β-Hz curve, and the analysis of the crystal alignment is in relation to these four reflections. In their curve, the large signal of more than 11,000 inputs at peak 38.23 exactly matches with identical peaks of pure protein molecules, such as trypsin and haemoglobin, which indicates that the arrangement of the β-Hz dimer produces a preferred orientation with perfect cubic symmetry. In addition, the crystallographic data according to the indexing software of the CDCC database produce different interplanar distances and space groups. The crystal habit and cell parameters for β-Hz show two crystalline systems (monoclinic and tetragonal), another two for the faeces sample (monoclinic and orthorhombic) and another (orthorhombic) for Hz alone, as recorded in Table II.

Crystallographic Data

It is interesting to see how the strong peak at 27.60 (3,996) observed in the faeces sample appears in Hz at 28.03 and 28.69 peaks; whereas for

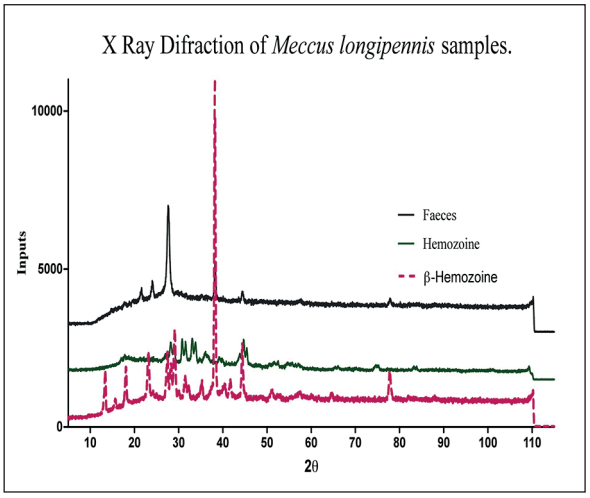

Figure 7. XRD patterns comparison of Hz, β-Hz and faeces. The 2θ rank was 12° to 102°, with Cobalto radiation (CoKα1=1.540560 A°). Reflection maximum values at 2Θ (°) and [inputs]. The curves have vertical displacement for better view. Faeces: 21.61, 24.01 (1,623), 27.60 (3,996), 38.20 (2,051), 44.28 (1,165), 77.77. Hz: 28.03, 28.69, 30.69 (1,253), 31.44, 32.97 (1,222), 33.65, 44.63 (1,166), 45.26. β-Hz: 13.29 (1,769), 18.01 (1,861), 23.08 (2,377), 27.37 (2,344), 28.19, 29.08 (3,042), 38.23 (11,054), 44.38 (2,640), 77.71. Hemoglobin and trypsin samples were observed with face cubic center patterns, with only four peaks and (inputs): 38.33 (11,472), 44.47 (2,919), 64.55 (752) and 77.68 (1,590) (data not showed).

Table II. Crystallographic data of Hz and ß-Hz from *Meccus longipennis*.

d [Å]/Calculated value	h	k	l	Mult.	Space group	Crystal system	Cell parameters
ß-Hemozoine M.l.							
6.5864	1	1	0	4	C 1 c 1 (9)	++Monoclinic	a=19.6441 Å b=7.0958 Å c=18.7029 Å β=115.692º
3.2040	0	2	1	4	P 1 21/m 1 (11)	Monoclinic	a=12.1011 Å b=8.5290 Å c=4.8841 Å β=96.240º
3.9265	1	1	0	4	I 4/m (87)	Tetragonal	a=5.5529 Å c=7.8993 Å
4.9705	2	0	0	2	P 1 21/c 1 (14)	Monoclinic	a=10.6776 Å b=6.9148 Å c=14.1193 Å β=111.407º
Faeces M.l.							
3.2142	1	3	0	4	P 1 21/m 1 (11)	Monoclinic	a=5.4350 Å b=12.2410 Å c=6.9320 Å β=106.260º
2.3488	2	2	0	6	P b c a (61)	Orthorhombic	a=35.2450 Å b=7.7757 Å c=7.1720 Å
Hemozoine M.l.							
3.2421	6	2	0	4	P b c a (61)	Orthorhombic	a=35.2450 Å b=7.7757 Å c=7.1720 Å
Haemoglobine® B&D and Trypsine® Sigma							
2.3435/2.3480	1	1	1	8	F m-3 m (225)	Cubic	a=4.0590 Å
2.0295/2.0353	2	0	0	6			
1.435 /1.4405	2	0	2	12			
1.2238/1.2261	3	1	1	24			
1.1717	2	2	2	8			
1.0148	4	0	0	6			

β-Hz, the strong peak is divided into 27.37, 28.19 and 29.08. However, the large peak at 38.23 that is present in the β-Hz and faeces samples do not appear in purified Hz. This means that in the natural faeces sample, there is also a face cubic centre in the cubic system (4 and 6) corresponding to iron from β-haemozoin; therefore, both samples are identical. However, Hz presents a different orthorhombic crystalline structure, as recorded in Table II. In both molecules, reflection peaks corresponding to aromatic compounds, such as $C_6H_8N_2$ [00-004-0258], with signals at 33.75, 38.85 and 55.18, and inorganic Fe_3N [01-073-2101], with signals at 80.5, 92 and 103.56, were observed. Even though there is a non-coincident peak at approximately 67°, these results apparently indicate a different crystalline structural characteristic, which also confirms that it is a natural material with a high purity grade and demonstrates an adequate procedure for obtaining the material.

It is important to note that some references[28,29] mention that synthetic β-haematin crystals can be produced *in vitro* with the same nuclear magnetic resonance and X-ray diffraction patterns as the haemozoin of the malaria parasite by adding a whole trophozoite lysate that has been acidified to a pH between 5 and 6. However, there are still differences between synthetic and natural haemozoin (sHz & nHZ), for example, the size and shape of the crystals may not be identical due to differences in the purification process that is used. Natural haemozoin is composed of small crystals measuring between 50 nm and 500 nm, and synthetic β-haematin crystals can range from 50 nm to 20 μm, depending on the solvent used[28,29]. Other results[30,31] illustrate that the haem aggregates, which are precipitated by these systems, need to be carefully scrutinized, especially by powder diffraction, to ensure that the malaria pigment is present in the purest state. Finally, our methodology is efficient, safe and effective, producing good material obtained from the natural faecal material of blood-sucking insects; therefore, the preparation of biological cultures of the parasite (*plasmodium*) transmitter of the disease is not necessary[23] because we use them in this study as an alternative material for the evaluation of antimalarial drugs.

Antimalarial Voltammetry

Determining the redox response of medicines alone was necessary before studying the interaction between the antimalarial drugs and the Hz and β-Hz molecules.

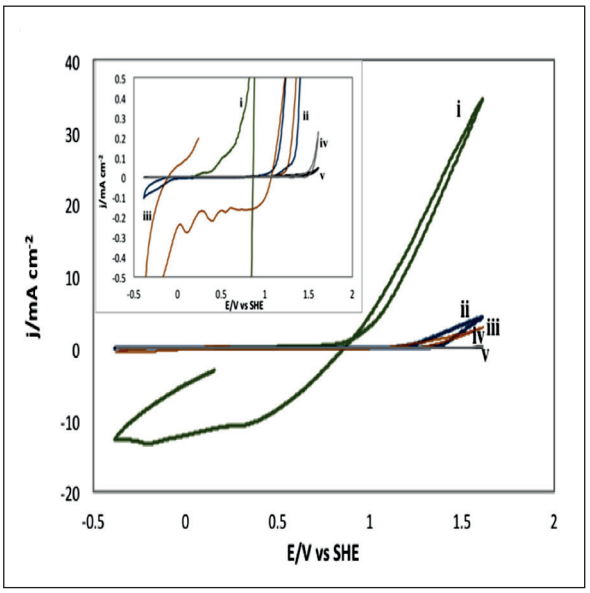

Figure 8. CV on CPE-AQ (*green curve, i*), CPE-CQ (*blue curve, ii*), CPE-QN (*orange curve, iii*), CPE-ART (*gray curve, iv*) and CPE-LF (*black curve, v*) in the anodic direction in a 0.15 M NaCl medium at pH 6.5 (v= 20 mvs^{-1}).

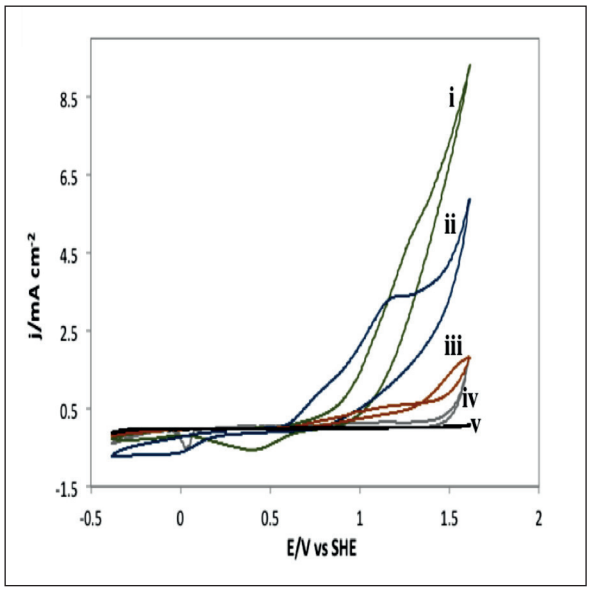

Figure 9. CV of CPE-AQ-Hz (*green curve, i*), CPE-CQ-Hz (*blue curve, ii)*, CPE-QN-Hz (*orange curve, iii*), CPE-ART-Hz (*gray curve, iv*) and CPE-LF-Hz (*black curve, v*).

Figure 8 shows the respective voltammograms in the anodic direction in a NaCl medium and shows different oxidation current densities (curves i, ii, iii, iv and v). At the same oxidation potential of 1.3 V current densities of 23 mAcm^{-2}, 4.8 mAcm^{-2}, 1 mAcm^{-2}, 0.009 mAcm^{-2} and 0.004 mAcm^{-2} for AQ, CQ, QN, LF and ART are produced, respectively. The decrease in the oxidation current density can be attributed to 1) the chemical nature of the drugs generating a less oxidizing environment or 2) the drugs diverting the oxidation processes of graphite and the medium to more anodic potentials. With these considerations, lumefantrine and artemether have the weakest oxidizing environment.

It is important to mention that the voltammetric response of all drugs in the cathodic direction is equal or similar to the anodic direction, which may indicate that all of them are found in a relative redox equilibrium or are not inert substances.

Voltammetry of Antimalarials Mixed with Hz

Due to the importance of the oxidation response in the generation of reactive oxygen species (ROS), which are the cause of damage to various biological molecules, we presented only those results related to anodic behavior.

Figure 9 shows five curves i, ii, iii, iv, and v of the CPE-Hz from *M. longipennis* in the presence of each drug. It can be seen that at the same oxidation potential of 1.3 V the current densities decrease with values at 5 mAcm^{-2}, 3.3 mAcm^{-2}, and 0.6 mAcm^{-2} for AQ, CQ, and QN, respectively, and the current densities increase with values at 0.15 mAcm^{-2} and 0.025 mAcm^{-2} for ART and LF, respectively. In this last case, the highest oxidizing power when Hz is present is for lumefantrine and artemether. When compared with the drugs alone (Figure 8), the results indicate that antimalarials *per se* can contribute to the oxidation processes and, in combination, can also increase or decrease the oxidizing power of Hz.

Voltammetry of Antimalarials Mixed with β-Hz

In the case of β-Hz combined with five drugs (Figure 10), it is possible to observe that the oxidation current densities majorly decrease with values at 2.8 mA cm^{-2} and 1.8 mA cm^{-2} for AQ and CQ, respectively; QN stays at the same value of 0.6 mA cm^{-2} for and low values of 0.03 mA cm^{-2} and 0.03 mA cm^{-2} are observed for ART and LF, respectively. It is very interesting that the lowest oxidizing power is for lumefantrine and artemether. In this respect, it seems that antimalarials can also be adjuvants to the oxidation processes and attenuate the oxidizing power.

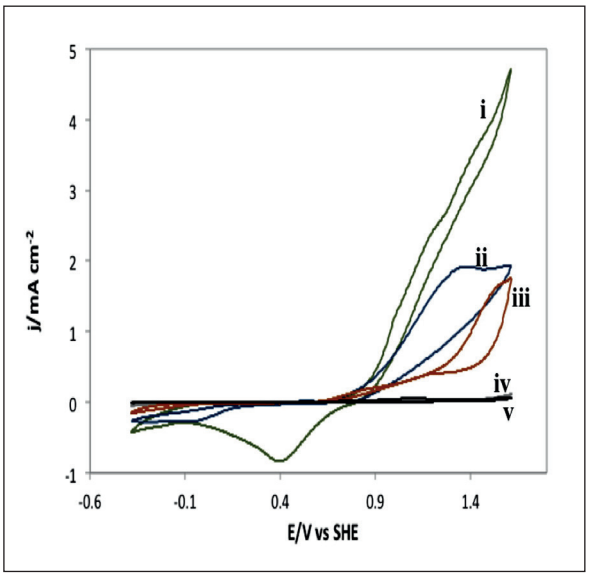

Figure 10. CV of CPE-AQ-β-Hz (green curve, i), CPE-CQ-β-Hz (blue curve, ii), CPE-QN-β-Hz (orange curve, iii), CPE-ART-β-Hz (gray curve, iv) and CPE-LF-β-Hz (black curve, v).

It is important to note that the oxidation current density, for a potential of 1.3 V with Hz-AQ and Hz-CQ are higher than those with β-Hz-AQ and β-Hz-CQ. These results are similar to assays of Hz and β-Hz without drugs and indicate that the most reactive molecule is Hz[7,21,22]. The β-Hz in the presence of drugs also has oxidizing power, and these are contradictory results. It is assumed that β-Hz is an inert molecule, which is formed by the parasite so that it does not suffer damage by the haem group, once the haem group is dimerized and "polymerized".

It has been demonstrated that both molecules are indeed "true" p-p dimers (pi bonds), and in this case, variable electronic transfers occur depending on which drugs can be employed, according to the recent theories of chemical and electronic bonding[32,33].

Voltamperometric Study of Hz and β-Hz With Lumefantrine and Artemether at Variable Concentrations

A mixed preparation of antimalarials, to check the stability of the redox potential, was conducted for a recommended treatment with the drug AL® [Coartem; Novartis, tablet contains 20 mg artemether and 120 mg lumefantrine (proportion 1:6)]. In this six-day treatment, the total dose administered was 0.480 g plus 1.920 g[34,35]. In this manner, the reactivity of haemozoin and β-haemozoin with lumefantrine and artemether in three different proportions can be viewed in Figures 11A, 11B, 11C and 11D. The varying weight ratios are listed in the following: graphite 2, 2.94, 3.84/Hz or β-Hz 1, 1, 1/drug 1, 1.94, 2.84, respectively.

Figures 11A and 11B show that there is a minor modification in the oxidation current densities of Hz with variable amounts of lumefantrine (electrophilic molecule with 3 chlorides directly influencing the pi bond of a benzene ring) and with variable amounts of artemether. In the β-Hz case Figures 11 (c) and (d), there are probably major modifications of the oxidation current densities with lumefantrine, but there are also those with artemether. In general, a drug ratio of 50:25:25 is very stable because the increase in drug no longer contributes to the oxidizing power of the artemether without aromatic groups (no pi bonds), which can interact with the p-p bond of Hz. The drug that decreases the oxidizing power of Hz the most is lumefantrine since for the same oxidation potential of 1 V, a low oxidation current density is obtained with respect to the artemether drug (0.02 $mAcm^{-2}$ and 0.09 mA cm^{-2}, respectively).

Discussion

The mechanism of action of artemisinin (ART) drugs is still under debate, but a widely held view is that ART is a pro-drug that is activated by reductive cleavage of an endoperoxide ring; the resulting free radical is thought to react with susceptible groups within a range of essential parasite proteins, thus leading to cellular damage and death[36-38]. Direct insights into the nature of the ART activator *in vivo* is unknown, but some studies suggest that it is important to maintain redox homeostasis. The major disadvantage of ART drugs is that they have very short half-lives *in vivo* (0.5-2 hours). Indeed, it has been suggested that one reason for the short half-lives of endoperoxide antimalarials is premature opening of the endoperoxide ring when the drug is located away from the active site in the parasite[37].

The crystalline structure of haemozoin shows the presence of dimers stabilized by p-p interactions that are also present in solution and have been proposed as an alternative nucleation unit. So, the beginning of haemozoin nucleation in the detoxification process requires the internal lipid membrane of the digestive vacuole[17-19] and an efficient proton pump that acidifies it[39]. These

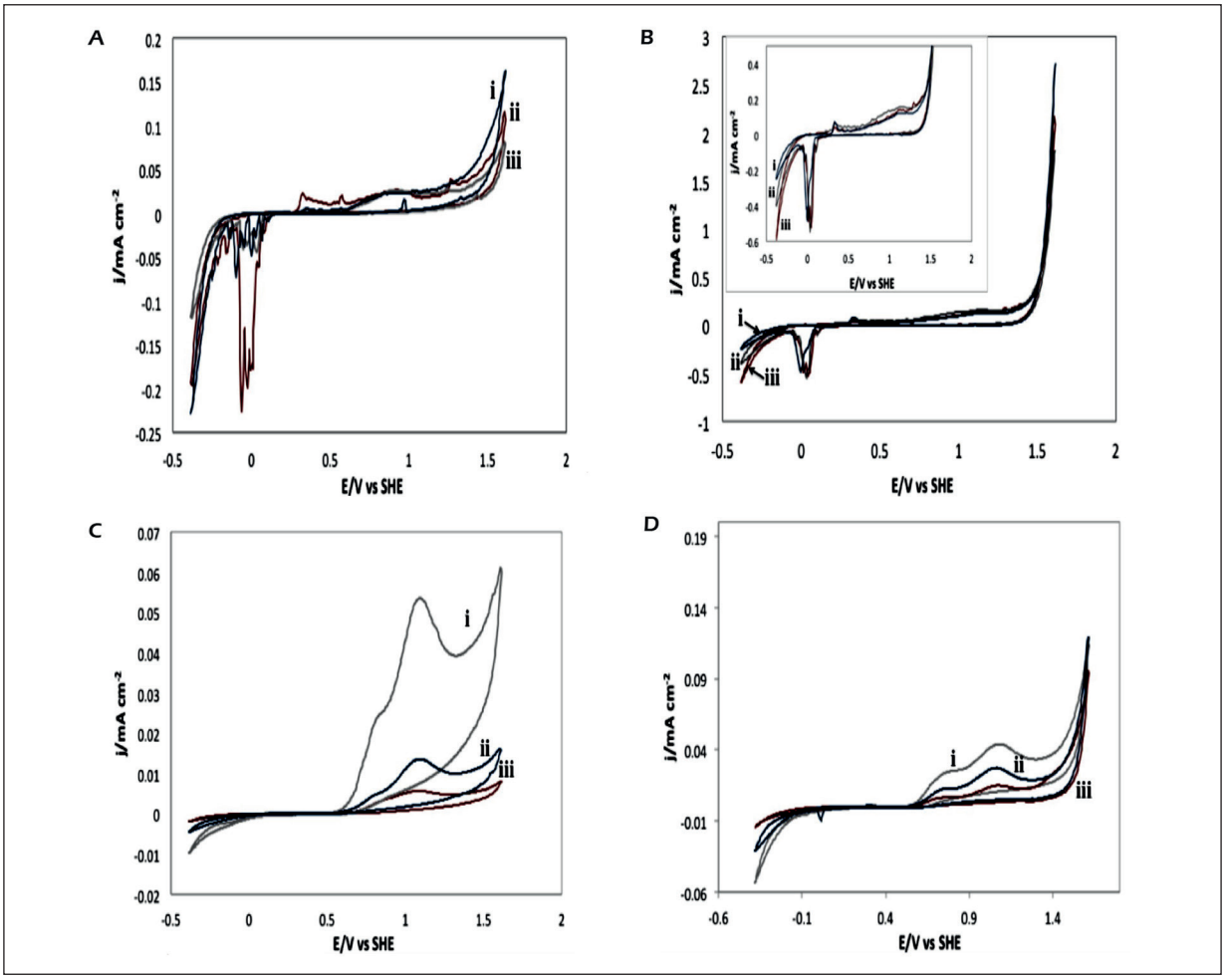

Figure 11. The four trials had the same proportions 50:25:25 (*blue curve, i*), 50:17:33 (*brown curve, ii*), and 50:13:37 (*gray curve, iii*) and were with anodic direction on NaCl medium 0.15 M, pH 6.6 (v= 20 mvs^{-1}).

nano-nuclear structures support the mechanism of action of antimalarial drugs that inhibit the growth of haemozoin. Recent studies have shown that the direct observation of intact cells, in a vitrified state, (it means without fixation process) locates and guide the haemozoin crystallization inside the inner membrane of digestive vacuole, and preferably occurs in aqueous phase rather than in lipid phase and facing the membrane in the common orientation face ×100ý. In addition, the haemozoin crystals are clearly not engulfed in any lipid sphere; rather, it is proposed that the haemozoin crystals form on an acylglycerol lipid film adsorbed to the inner leaflet of the DV phospholipid membrane[17-19].

The common coexistence of these crystalline species in physiological deposits and the observation that the nucleus of a stone is often chemically different than the material in subsequent layers led Lonsdale[40] in 1968 to suggest that epitaxial relationships between these crystalline phases could be an important factor contributing to their formation. Epitaxy is defined as the growth of one crystal on the substrate of another, so there is at least one preferred orientation and a near geometrical fit between the contacting surface lattices[41]. When lattice-matched "seeds" are present in solution, the barrier to nucleation can be significantly reduced, so crystallization occurs in environments that have otherwise not met critical supersaturating conditions. A similar scene may be present for haemozoin and antimalarial drugs.

Quinolines also form various complexes with soluble haematin, but complexation is insufficient to suppress haem detoxification and is a poor indicator of drug specificity.

The divergent hypotheses on the inhibition of haematin crystallization posit that drugs act

either by the sequestration of soluble haematin by forming non crystallizable complexes or the inhibition is due to the drug interaction with crystal surfaces. However, drug-crystal interactions are not the dominant mechanism of haematin growth inhibition[42].

The redox potential variability from insoluble and nonconductive organic molecules, such as Hz and β-Hz in the presence of antimalarial drugs has been quantified through an electrochemical array with a carbon paste electrode (CPE).

Finally, the authors have shown the viability of conducting quantitative characterization studies of insoluble drugs, such as antimalarial artemether and lumefantrine using cyclic voltammetry with carbon paste electrodes in a fast and inexpensive manner; furthermore, this technique is able to consider the more complex planar aromatic structures and the presence of fluorine and chlorine, which are very electronegative atoms.

Conclusions

Clinically, the toxicity and side effects of artemether and lumefantrine are presents. Some patients complained of dizziness, headache, nausea, vomiting, abdominal, pain, diarrhoea, and palpitation. A few patients had rashes and others had reticulopenia, leukopenia, and increased SGPT, and urea nitrogen, sinus bradycardia, arrhythmia or premature ventricular beat. To maintain the intracellular redox balance is very important, so indicate treatments that could potentially alter it, (artemether) or (benflumetol,) should consider that maybe there will be a imbalance. A better guide for rational application and standardize malaria treatment should be include to evaluate the drugs redox potential[43].

Conflict of Interest

The Authors declare that they have no conflict of interests.

Acknowledgements

To the Ministry of Public Education (SEP-PROMEP: Secretaría de la Educación Pública-Programa de Mejora del Profesorado) for the financial support to Biomedical Research Academic Group, in the 2013 call for Consolidate Research Groups. The authors would like to acknowledge and truly thank the collaboration of *Yesenia Elizabeth Ruvalcaba Cobián* who holds a B.A in Teaching English as a Foreign Language, for her contributions on the revision and translation of the article.

Authors' Contribution

J.L. Imbert Palafox designed and directed the project and wrote the final manuscript. L. González Linares made the experimental materials and did the Voltammetry assays. V.E. Reyes-Cruz conducted and demonstrated the management and use of the Voltammeter. A. Arenas Flores conducted and analyzed the XRD equipment and its respective software. J.E. Bautista Garcia prepared and cultivated the insect's colony and C.M. Gonzalez Alvarez made the spectrophotometric assays. M.A. Becerril Flores and J.C. Ruvalcaba Ledezma read and re-wrote the initial manuscript. All authors read and agree on the submitted version of the manuscript.

References

1) Thomas V, Góis A, Ritts B, Burke P, Hänscheid T, McDonnell G. A novel way to grow hemozoin-like crystals in vitro and Its use to screen for hemozoin Inhibiting Antimalarial Compounds. PLoS One 2012; 7: e41006.
2) Slomianny C. Three-dimensional reconstruction of the feeding process of the malaria parasite. Blood Cells 1990; 16: 369-378.
3) Rosenthal PJ, Meshnick SR. Hemoglobin catabolism and iron utilization by malaria parasites. Mol Biochem Parasitol 1996; 83: 131-139.
4) Abu Bakar N, Klonis N, Hanssen E, Chan C, Tilley L. Digestive-vacuole genesis and endocytic processes in the early intraerythrocytic stages of Plasmodium falciparum. J Cell Sci 2010; 123: 441-450.
5) Sullivan DJ Jr, Guzman IY, Goldberg DE. Plasmodium hemozoin formation mediated by histidine-rich proteins. Science 1996; 271: 219-22.
6) Stiebler R, Timma BL, Oliveira PL, Hearne GR, Egan TJ, Oliveira MF. On the physico-chemical and physiological requirements of hemozoin formation promoted by perimicrovillar membranes in Rhodnius prolixus midgut. Insect Biochem Mol Biol 2010; 40: 284-292.
7) Goldberg DE, Slater AFG, Cerami A, Henderson GB. Hemoglobin degradation in the malaria parasite plasmodium falciparum: an ordered process in a unique organelle. PNAS 1990; 87: 2931-2935.
8) Kollien AH, Schaub GA. The development of Trypanosoma cruzi in Triatominae. Parasitology Today 2000; 16: 381-387.
9) Caiaffa CD, Stiebler R, Oliveira MF, Lara FA, Paiva-Silva GO, Oliveira PL. Sn-protoporphyrin inhibits both heme degradation and hemozoin formation in Rhodnius prolixus midgut. Insect Biochem Mol Biol 2010; 40: 855-860.
10) Oliveira MF, Silva JR, Dansa-Petretski M, de Souza W, Lins U, Braga CMS, Masuda H, Oliveira PL. Haem detoxification by an insect. Nature 1999; 400: 517-518.

11) Oliveira MF, Silva JR, Dansa-Petretski M, de Souza W, Braga CMS, Masuda H, Oliveira PL. Haemozoin formation in the midgut of the blood-sucking insect Rhodnius prolixus. FEBS Lett 2000; 477: 95-98.

12) Oliveira MF, d'Avila JCP, Torres CR, Oliveira PL, Tempone AJ, Rumjanek FD, Braga CMS, Silva JR, Petretski MD, Oliveira MA, de Souza W, Ferreira ST. Haemozoin in Schistosoma mansoni. Mol Biochem Parasitol 2000; 111: 217-221.

13) Chen MM, Shi L, Sullivan DJ, Jr. Haemoproteus and Schistosoma synthesize heme polymers similar to Plasmodium hemozoin and beta-hematin. Mol Biochem Parasitol 2001; 113: 1-8.

14) Oliveira MF, Kycia SW, Gomez A, Kosar AJ, Bohle DS, Hempelmann E, Menezes D, Vannier-Santos MA, Oliveira PL, Ferreira ST. Structural and morphological characterization of hemozoin produced by Schistosoma mansoni and Rhodnius prolixus. FEBS Lett 2005; 579: 6010-6016.

15) Oliveira MF, Timm BL, Machado EA, Miranda K, Attias M, Silva JR, Petretski, de Oliveira MA, de Souza W, Pinhal NM, Souza JJF, Vugman NV, Oliveira PL. On the pro-oxidant effects of haemozoin. FEBS Lett 2002; 512: 139-144.

16) Graça-Souza, AV, Maya-Monteiro C, Paiva-Silva GO, Braz GR, Paes MC, Sorgine MH, Oliveira MF, Oliveira PL. Adaptations against heme toxicity in blood-feeding arthropods. Insect Biochem Mol Biol 2006; 36: 322-335.

17) Kapishnikov S, Berthing T, Hviid L, Dierolf M, Menzel A, Pfeiffer F, Als-Nielsen J, Leiserowitz L. Aligned hemozoin crystals in curved clusters in malarial red blood cells revealed by nanoprobe X-ray Fe fluorescence and diffraction. PNAS 2012; 109: 11184-11187.

18) Kapishnikov S, Weiner A, Shimoni E, Guttmann P, Schneider G, Dahan-Pasternak N, Dzikowski R, Leiserowitz L, Elbaum M. Oriented nucleation of hemozoin at the digestive vacuole membrane in Plasmodium falciparum. PNAS 2012; 109: 11188-11193.

19) Kapishnikov S, Weiner A, Shimoni E, Schneider G, Elbaum M, Leiserowitz L. Digestive vacuole membrane in plasmodium falciparum-infected erythrocytes: relevance to templated nucleation of hemozoin. Langmuir 2013; 29: 14595-14602.

20) Vincent SH. Oxidative effects of heme and porphyrins on proteins and lipids. Semin Hematol 1989; 26: 105-113.

21) Rifkind JM, Nagababu E, Ramasamy S, Ravi LB. Hemoglobin redox reactions and oxidative stress. Redox Rep 2003; 8: 234-237.

22) Reyes CVE, Urbano GR, Veloz RMA, Imbert PJL. Analysis of the electrochemical reactivity of natural hemozoin and β-hemozoin in the presence of antimalarial drugs. Electrochim Acta 2011; 56: 9762-9768.

23) González LL, Reyes CVE, Velóz RMA, Urbano RG, Imbert PJL, Cobos MJA. New Method of Production and Characterization of Haemozoin and ß-Haemozoin from Meccus longipennis. Iran J Parasitol 2019; 14: 59-67.

24) Slater AFG, Cerami A. Inhibition by chloroquine of a novel haem polymerase enzyme activity in malaria trophozoites. Nature 1992; 355: 167-169.

25) Slater AFG, Swiggard WJ, Orton BR, Flitter WD, Goldberg DE, Cerami A, Henderson GB. An iron-carboxylate bond links the heme units of malaria pigment. PNAS 1991; 88: 325-329.

26) Bendrat K, Berger BJ, Cerami A. Haem polymerization in malaria. Nature 1995; 378: 138-139.

27) Olliaro PL, Goldberg DE. The plasmodium digestive vacuole: metabolic headquarters and choice drug target. Parasitology Today 1995; 11: 294-297.

28) Coronado LM, Nadovich CT, Spadafora C. Malarial hemozoin: from target to tool. Biochim Biophys Acta 2014; 1840: 2032-2041.

29) Egan TJ, Chen JY, de Villiers KA, Mabotha TE, Naidoo KJ, Ncokazi KK, Langford SJ, McNaughton D, Pandiancherri S, Wood BR. Haemozoin (beta-haematin) biomineralization occurs by self-assembly near the lipid/water interface. FEBS Lett 2006; 580: 5105-5110.

30) Vekilov PG, Rimer JD, Olafson K, Ketchum M. Lipid or aqueous medium for hematin crystallization? Cryst Eng Comm 2015; 17: 7790-7800.

31) Bohlea DS, Kosara AD, Stephens PW. Phase homogeneity and crystal morphology of the malaria pigment ß-hematin. Acta Crystallogr 2002; 58: 1752-1756.

32) Kapetanaki S, Varotsis C. Ferryl-oxo heme intermediate in the antimalarial mode of action of artemisinin. FEBS Lett 2000; 474: 238-241.

33) Webster GT, Tilley L, Deed S, McNaughton D, Wood BR. Resonance Raman spectroscopy can detect structural changes in haemozoin (malaria pigment) following incubation with chloroquine in infected erythrocytes. FEBS Lett 2008; 582: 1087-1092.

34) Khandave, SS, Joshi, SS, Sawant, SV and Onkar, SV. Evaluation of bioequivalence and cardio-hepatic safety of a single dose of fixed dose combination of artemether and lumefantrine. J Bioequivalence Bioavailab 2010; 2: 081-085.

35) World Health Organization. Guidelines for the treatment of malaria. WHO/Global Malaria Program. Information Note on Delayed Haemolytic Anaemia following Treatment with Artesunate, 2 October 2013. https://www.who.int/malaria/publications/atoz/who_note_delayed_haemolytic_anaemia_oct13.pdf?ua=1 [cited 2019, March 9].

36) Loup C, Lelievre J, Benoit-Vical F, Meunier B. Trioxaquines and heme-artemisinin adducts inhibit the in vitro formation of hemozoin better than chloroquine. Antimicrobial Agents Chem 2007; 51: 3768-3770.

37) Chen Y, Zheng J, Zhu S, Chen H. Evidence for hemin inducing the cleavage of peroxide bond or artemisinin (Qinghaosu): cyclic voltammetry and in situ FT IR spectroelectrochemical studies on the reduction mechanism of artemisinin in the presence of hemin. Electrochim Acta 1999; 44: 2345-2350.

38) Klonis N, Darren JC, Tilley L. Iron and heme metabolism in Plasmodium falciparum and the mechanism of action of artemisinins. Curr Opin Microbiol 2013; 16: 722-727.

39) Ginsburg H. Abundant proton pumping in Plasmodium falciparum, but why? Trends Parasitol 2002; 18: 483-486.

40) Lonsdale K. Epitaxy as a growth factor in urinary calculi and gallstones. Nature 1968; 217: 56-58.

41) Frincu, MC, Fogarty CE, Swift, JA. Epitaxial relationships between uric acid crystals and mineral surfaces: a factor in urinary stone formation. Langmuir 2004; 20: 6524-6529.

42) Olafson KN, Nguyen TQ, Rimer JD, Vekilov PG. Antimalarials inhibit hematin crystallization by unique drug-surface site interactions. PNAS 2017; 114: 7531-7536.

43) Chang Ch. Development of antimalarial drugs and their application in China: a historical review. Infect Dis Poverty 2014; 3: 9.